nature chemistry

ARTICLES

https://doi.org/10.1038/s41557-018-0102-z

The energy-transfer-enabled biocompatible disulfide–ene reaction

Michael Teders[1], Christian Henkel[2], Lea Anhäuser[3], Felix Strieth-Kalthoff[1], Adrián Gómez-Suárez[1], Roman Kleinmans[1], Axel Kahnt[2], Andrea Rentmeister[3,4], Dirk Guldi[2*] and Frank Glorius[1*]

Sulfur-containing molecules participate in many essential biological processes. Of utmost importance is the methylthioether moiety, present in the proteinogenic amino acid methionine and installed in tRNA by radical-*S*-adenosylmethionine methylthiotransferases. Although the thiol–ene reaction for carbon–sulfur bond formation has found widespread applications in materials or medicinal science, a biocompatible chemo- and regioselective hydrothiolation of unactivated alkenes and alkynes remains elusive. Here, we describe the design of a general chemoselective *anti*-Markovnikov hydroalkyl/aryl thiolation of alkenes and alkynes—also allowing the biologically important hydromethylthiolation—by triplet–triplet energy transfer activation of disulfides. This fast disulfide–ene reaction shows extraordinary functional group tolerance and biocompatibility. Transient absorption spectroscopy was used to study the sensitization process in detail. The hereby gained mechanistic insights were successfully employed for optimization of the catalytic system. This photosensitized transformation should stimulate bioimaging applications and carbon–sulfur bond-forming late-stage functionalization chemistry, especially in the context of metabolic labelling.

Developing new reaction methodologies that give access to unprecedented reactivity modes or provide more selective, efficient and environmentally sustainable alternatives to established approaches is the central goal of many research programmes throughout chemistry[1]. Inspiration for the design of new reactions is rooted in the understanding of reaction mechanisms and the fundamental reactivity principles that underpin them[2]. Methylthioether functionalities, which are ubiquitous and of utmost importance in nature, are inserted into tRNA and ribosomal proteins by highly effective radical-*S*-adenosylmethionine (SAM) methylthiotransferases bearing [4Fe-4S] redox-active clusters (Fig. 1a)[3–5]. Surprisingly, the way that organisms construct carbon–sulfur bonds during the biosynthesis of sulfur-containing residues in living organisms is barely understood[5]. Thiyl radicals are essential intermediates in many biosynthetic pathways[6,7], for example, in the deoxygenation of ribonucleotides[8], a transformation occurring in living organisms as part of the de novo generation of DNA precursors. The omnipresence of thiyl radicals in biological systems[9] along with their various synthetic opportunities to access organosulfur moieties widely represented within natural products, pharmaceuticals or material products[10], has been an inspiration to investigate the utilization of these highly reactive species in diverse applications[11]. Thiol–ene click reactions[12], in which a thiyl radical generated from the corresponding thiol regioselectively adds in an *anti*-Markovnikov fashion to an alkene, are among the most prominent approaches to carbon–sulfur bond formation[13]. They have been applied in bioconjugates[14,15], pharmaceutical chemistry[16] and polymer science[17]. In the past, UV-light irradiation or radical initiators have mostly been used for the generation of thiyl radicals[11]. However, the functional group tolerance, the need for costly set-ups for UV irradiation and the production of huge amounts of waste have been limiting factors.

The aforementioned drawbacks set up the development of visible-light photocatalytic systems as a means to initiate the thiol–ene reaction (Fig. 1b)[18–20]. Significantly milder reaction conditions of photocatalytic systems enable application in bioconjugation reactions and polymer synthesis[21,22]. Despite such advantages, the photoinitiated thiol–ene reaction still suffers from three major limitations. First, the inherent reactivity of thiols (for example, thiol–Michael additions) goes hand-in-hand with a lack of chemoselectivity, especially in complex molecules bearing suitable Michael acceptor functionalities[23]. Second, the hydromethylthiolation of unactivated alkenes and alkynes under mild and biocompatible conditions has never been reported, due to the need to handle highly toxic, gaseous methanethiol as reagent. Third, a chemoselective generation of thiyl radicals from thiols in biological systems is hardly possible due to the presence of cellular thiols, limiting the overall value of this approach for labelling applications.

Inspired by the S–S bond dissociation energies of aliphatic disulfides of ~65 kcal mol^{-1} (ref. [24]), reports on the direct sensitization of aryl disulfides using UV light[11], and the mild reaction conditions of a sensitization protocol, we hypothesized using suitable photocatalysts for the energy transfer activation of alkyl disulfides, such as dimethyl disulfide (**2**), to access alkylthiyl radicals (Fig. 1c)[25]. This energy-transfer-enabled disulfide–ene reaction would allow the biologically relevant chemoselective hydromethylthiolation of alkenes and alkynes under mild conditions, namely visible-light irradiation[26,27]. The use of visible light as an abundant natural resource to promote chemical reactions offers many advantages[28]. Considering the costs and environmental sustainability, photocatalytic reactions have attracted widespread attention, with many examples demonstrating unusual or exotic reactivity patterns that do not occur in the absence of light[29,30]. Ground-breaking transformations utilizing photoexcited catalysts to engage in electron transfer processes with organic molecules or other metal complexes have been achieved recently[29–31]. The other fundamental pathway for the bimolecular decay of photoexcited states, namely energy transfer,

[1]Organisch-Chemisches Institut, Westfälische Wilhelms-Universität Münster, Münster, Germany. [2]Department für Chemie und Pharmazie, Friedrich-Alexander-Universität Erlangen-Nürnberg, Erlangen, Germany. [3]Institut für Biochemie, Westfälische Wilhelms-Universität Münster, Münster, Germany. [4]Cells-in-Motion Cluster of Excellence (EXC1003-CiM), Westfälische Wilhelms-Universität, Münster, Germany. *e-mail: dirk.guldi@fau.de; glorius@uni-muenster.de

has rarely been used in organic synthesis[29]. Triplet–triplet energy transfer (TTEnT) from visible-light photocatalysts has only been utilized to achieve a small number of organic transformations[29]. These are roughly divided into three categories: *E*/*Z* isomerization of (activated) alkenes[32], [2+2] photocycloadditions[33,34] and sensitization of transition metal complexes[35].

Results and discussion

Luminescence screening and optimization. We began our studies with a hypothesis-driven approach by applying our recently reported luminescence quenching screening[36,37] to investigate the ability of dimethyl disulfide (**2**) to interact with various excited-state photocatalysts featuring different excited-state triplet energies. In particular, four different Ir-based photocatalysts gave rise to significant luminescence quenching when dimethyl disulfide (**2**) is present. The photocatalyst [Ir(dF(CF$_3$)ppy)$_2$(dtbbpy)](PF$_6$) (**[Ir–F]**, dF(CF$_3$)ppy = 2-(2,4-difluorophenyl)-3-trifluoromethylpyridine, dtbbpy = 4,4′-di-*tert*-butyl-2,2′-bipyridine) was the most efficient among them, with a quenching fraction of 42% (Fig. 2a). The luminescence quenching correlated with the triplet excited-state energies of the photosensitizers. Notably, catalysts with exceptionally high excited-state oxidation or reduction potentials showed no or lower luminescence quenching. From this we assume that a TTEnT reaction from the excited photocatalyst to the disulfide is the modus operandi.

To investigate the chemo- and regioselectivity of the hydromethylthiolation reaction, carvone (**1a**), dimethyl disulfide (**2**) and **[Ir–F]** were reacted in acetonitrile under visible-light irradiation (λ_{max} = 455 nm). Of great relevance is the fact that the yield of the methylthiolated product **3a** correlated perfectly with the screening results. Due to the electrophilic nature of the methylthiyl radical, the exocyclic, more electron-rich alkene functionality of carvone (**1a**) was chemo- and regioselectively hydromethylthiolated in an *anti*-Markovnikov fashion (Fig. 2a). Our TTEnT activation hypothesis was independently supported by control reactions, in which the need for the **[Ir–F]** photosensitizer and light were demonstrated. To further support this hypothesis, benzophenone, a classical triplet sensitizer, was used under 365 nm irradiation, affording the desired product **3a** in 25% yield. Further optimization of parameters, such as the irradiation wavelength or the solvent, allowed the yield of **3a** to be increased to 74% (Supplementary Section 3.1). The reaction is characterized by a fast reaction progress, as documented in the reaction profile (Fig. 2b).

Substrate scope and limitations. With the optimized reaction conditions in hand, we investigated the scope and synthetic limitations of this disulfide–ene reaction (Fig. 3). The hydromethylthiolation of alkenes tolerates a wide range of functional groups, such as ketones (**3b**), aldehydes (**3c**), epoxides (**3f**, **3v**), amides (**3g**, **3w**), alcohols (**3h**, **3p**), nitriles (**3r**), esters (**3l**, **3t**), sulfonamides (**3x**) or heterocycles (**3i**, **3k**, **3w**, **3x**). In all cases, the corresponding products are formed in moderate to good yields (42–85%). Substrates exhibiting more than one unsaturated carbon–carbon bond are chemoselectively methylthiolated in an *anti*-Markovnikov fashion at the more electron-rich, sterically more easily accessible alkene functionality. Aliphatic disulfides with longer alkyl chains (**3y** and **3z**) or with a hydroxy group (**3aa**) could also be employed using this protocol, whereas in the case of sterically demanding disulfides, such as *tert*-butyl disulfide, no reactivity is observed (**3ab**; Supplementary Section 4.11). A slight modification of the reaction conditions allows the use of diaryl disulfides as thiyl radical precursors for the synthesis of arylthioethers (**3ac**–**3ae**, 84–89%). Furthermore, the functionalization of an azide derivative (**3af**) and of amino acids (**3ag**–**3ai**) as bioconjugates delivers the respective hydrothiolated products in good yields, paving the road for potential in vitro and in vivo applications. The *vic*-di-methylthiolation of different alkynes

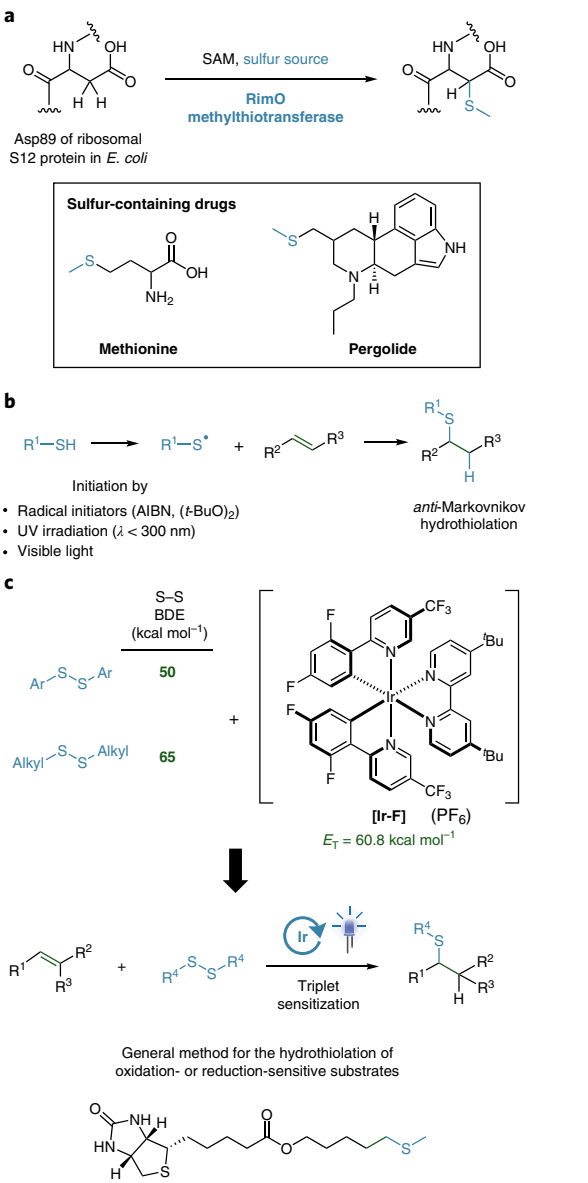

Fig. 1 | Chemoselective *anti*-Markovnikov hydrothiolation of alkenes—allowing the biologically important hydromethylthiolation—enabled by triplet–triplet photosensitization of disulfides. a, Methylthioether scaffolds are involved in diverse biosynthetic processes. Furthermore, this functional unit can be identified in important drugs, such as in the essential amino acid methionine or in pergolide, an ergoline-based dopamine receptor agonist used for the treatment of Parkinson's disease. **b**, The photocatalytic thiol–ene click reaction allows carbon–sulfur bond formation under extremely mild conditions and is therefore widely used in bioconjugate chemistry, polymer science and pharmaceutical synthesis. However, this methodology is still limited by chemoselectivity issues and by oxidative or reductive reaction environments limiting the functional group tolerance of the overall reaction. The biologically important hydromethylthiolation is challenging, and biochemical applications are hardly possible due to the presence of cellular thiols participating in undesired side reactions. **c**, The design of a biocompatible energy-transfer-enabled disulfide–ene reaction would allow the chemo- and *anti*-Markovnikov selective construction of important methylthioethers. Triplet–triplet sensitization of disulfides by photocatalysts with sufficient triplet excited-state energy may allow the mild installation of alkyl- and arylthioether scaffolds. Tuning of the photocatalysts redox potentials would even allow the hydrothiolation of oxidation- or reduction-sensitive compounds. BDE, bond dissociation energy.

a

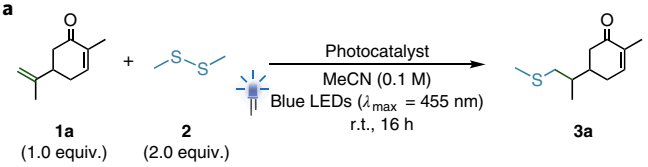

1a (1.0 equiv.) + **2** (2.0 equiv.) → **3a**

Photocatalyst	E_T (kcal mol^{-1})	$E_{1/2}^{II/III*}$ (V)	$E_{1/2}^{III*/IV}$ (V)	Quenching fraction *F*	Yield **3a** (%)
[Ir-F]	60.8	+1.21	−0.89	42	58
fac-[Ir(dF(ppy))$_3$]	59.1	+0.34	−1.44	24	53
[Ir(ppy)$_2$(NHC-F$_2$)]	57.8	+0.38	−1.49	31	47
fac-[Ir(ppy)$_3$]	57.8	+0.31	−1.73	19	46
[Ir(ppy)$_2$(dtbbpy)](PF$_6$)	49.2	+0.66	−0.96	<5	0
[Ru(bpz)$_3$](PF$_6$)$_2$	48.4	+1.45	−0.26	<5	0
[Ru(phen)$_3$](PF$_6$)$_2$	46.8	+0.82	−0.87	<5	0
[Ru(bpy)$_3$](PF$_6$)$_2$	46.5	+0.77	−0.81	<5	0

Increasing triplet excited-state energy

b

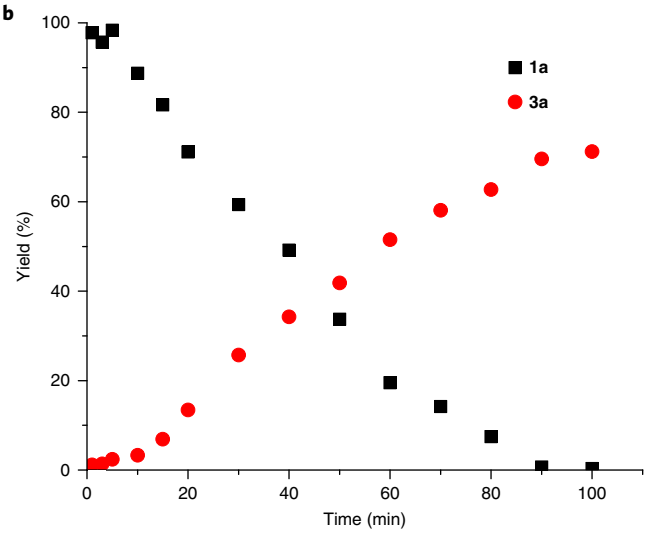

Fig. 2 | Hypothesis-driven luminescence screening and reaction profile of the chemoselective *anti*-Markovnikov disulfide–ene reaction. **a**, Mechanism-based luminescence quenching studies of dimethyl disulfide (**2**) and various photosensitizers reveal a correlation between quenching and the photocatalysts' triplet excited-state energy E_T (for details on luminescence quenching studies, see Supplementary Section 2.1). This trend was also observed in the hydromethylthiolation of the exocyclic alkene functionality of carvone (**1a**), presumably enabled by triplet–triplet sensitization of dimethyl disulfide (**2**) by the respective photocatalyst. All potentials are given in volts versus the saturated calomel electrode (SCE) and were measured in acetonitrile. **b**, Hydromethylthiolation of the exocyclic alkene functionality of carvone (**1a**) proceeds in a quick fashion without an induction period. The starting material is completely consumed within 90 min. The reaction profile was independently determined twice with similar results.

was successful, affording an *E*/*Z* mixture of **3aj** and **3ak** in 83% and 68% yield, respectively. The second methylthiolation event most probably occurs through reaction of the vinyl radical intermediate with a ground-state disulfide molecule as part of a chain reaction. The benzothiophene heterocycle **3al** could be regioselectively created when reacting diphenyl disulfide with 1-phenyl-prop-1-yne (73%)[38]. Various drug derivatives, incorporating a probenecid (**3am**), a dehydrocholic acid (**3an**), an estrone (**3ao**) or an erucic acid (**3ap**) scaffold, could be methylthiolated in good to excellent yields. Finally, the functional group tolerance and preservation of this reaction was analysed by performing additive-based robustness screens, indicating a high robustness and functional group preservation of the overall transformation (Supplementary Table 3)[39,40].

Mechanistic investigations. To corroborate the reaction mechanism and to support the postulated TTEnT, photosensitization of dimethyl disulfide (**2**) and/or 1-octene by **[Ir–F]** was studied in detail. Experiments showed that methyl(octyl)sulfane formation is based on irradiation with light (400 nm $< \lambda \leq$ 455 nm) and the presence of the photocatalyst. From steady-state UV–vis absorption spectroscopy we conclude that visible light (400 nm $< \lambda \leq$ 455 nm) is exclusively absorbed by the **[Ir–F]** photocatalyst and that neither **2** (λ_{max} = 255 nm) nor 1-octene (λ_{max} < 200 nm) is appreciably photoactivated (Fig. 4a). In other words, the photocatalyst is crucial in the visible-light-driven disulfide–ene reaction.

To shed light on the mechanistic aspects, phosphorescence quenching of **[Ir–F]** on addition of **2** and/or 1-octene was investigated by Stern–Volmer analyses: **2** is an effective phosphorescence quencher, while 1-octene is not at all. Our findings are in agreement with the screening results and suggest favourable interactions between **[Ir–F]** and **2** (Fig. 4b), but no interactions between **[Ir–F]** and 1-octene. Consequently, we characterized the nature of the **[Ir–F]**/(**2**) interaction. The triplet excited-state energies of **2** and **[Ir–F]** were determined using cryostatic phosphorescence measurements as 66.1 ± 2.2 and 60.8 ± 0.01 kcal mol^{-1}, respectively, suggesting a slightly endergonic activation of **2** by the **[Ir–F]** photocatalyst, a phenomenon that has been rarely described in the literature[41]. To examine the underlying kinetics, nanosecond time-resolved transient absorption spectroscopy (ns-TAS) was performed using **[Ir–F]** in the absence and presence of variable **2** concentrations reaching 9×10^{-2} M (Fig. 4c). The ns-TAS results for 387 nm photoexcited **[Ir–F]** are dominated by a rather broad 462 nm maximum. Based on literature reports, we ascribe the new transient to the excited triplet metal-to-ligand charge-transfer/ligand-centred (MLCT/LC) state of the **[Ir–F]** photocatalyst[42]. Its lifetime, which is 2.49 ± 0.06 µs in the absence of any **2**, is subject to a **2** concentration-dependent shortening. Concomitant with quenching of the **[Ir–F]** ^{3*}MLCT/LC transients, we observed the formation of newly developing transient absorption features at 400 and 440 nm, which we tentatively assign to ^{3*}**2**. Confirmation for our assignment came from ns-TAS photosensitization experiments with Michler's ketone (4,4′-bis(dimethylamino) benzophenone)—a well-known organic photosensitizer—rather than benzophenone (Supplementary Fig. 8). Here, the same 400 and 440 nm features emerged at the expense of the Michler's ketone triplet excited-state maxima at 415, 512 and 695 nm (ref. [43]). Turning to kinetic analysis of the TTEnT we consider the following sequence:

$$^{3*}\text{[Ir–F]} \xrightarrow{k_{GSR,[Ir-F]}} \text{[Ir–F]} \quad (1)$$

$$^{3*}\text{[Ir–F]} + 2 \xrightarrow{k_{TTEnT}} \text{[Ir–F]} + {}^{3*}2 \quad (2)$$

By virtue of the intrinsic ground-state recovery rate (k_{GSR}) of the ^{3*}MLCT/LC state of the **[Ir–F]** photocatalyst, the observed rate constant (k_{obs}) for the overall TTEnT is based on

$$k_{obs} = k_{GSR} + [2] \cdot k_{TTEnT} \quad (3)$$

Overall, a perfect linear relationship was confirmed in the corresponding ($k_{obs} - k_{GSR}$) versus [**2**] plots with a slope of (1.16 ± 0.01) × 10^7 M^{-1} s^{-1} (Supplementary Fig. 11). The slope correlates with the TTEnT rate constant k_{TTEnT}, while a sizeable intercept

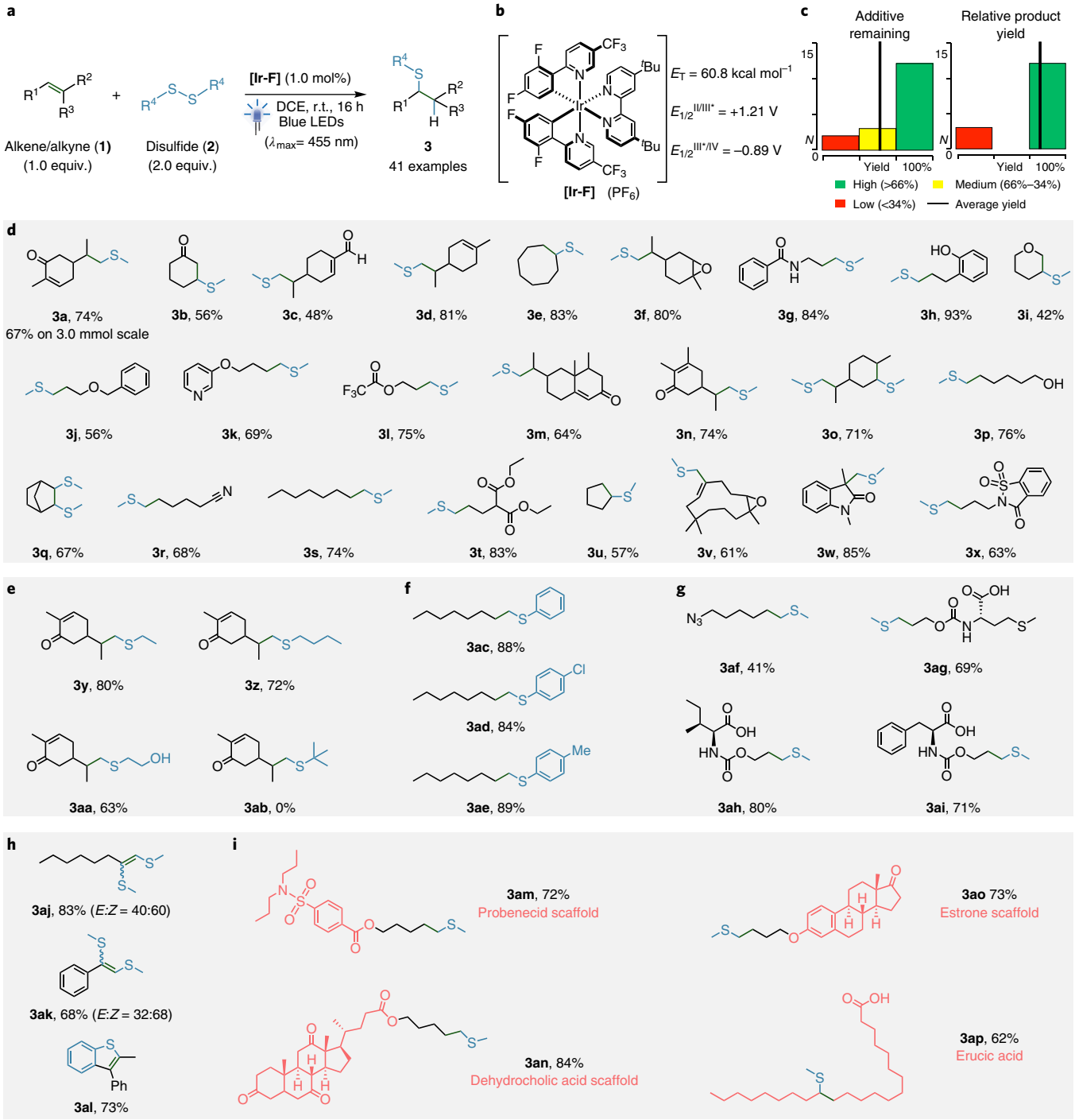

Fig. 3 | Scope of the disulfide–ene hydrothiolation of alkenes and alkynes. a, General reaction conditions used for scope preparation: alkene or alkyne (0.3 mmol, 1.0 equiv.), disulfide (0.6 mmol, 2.0 equiv.), **[Ir–F]** (0.003 mmol, 1.0 mol%), DCE (0.1 M), 455 nm, r.t., 16 h. **b**, Structure of the applied [Ir]-based photocatalyst and its photophysical properties. All potentials are given in volts versus SCE and were measured in acetonitrile. **c**, Results of an additive-based robustness screen corroborate a mild synthetic protocol. **d**, Hydromethylthiolation of diverse alkenes exhibiting different electronic and steric properties. Substrates exhibiting more than one unsaturated carbon–carbon bond are exclusively hydrothiolated at the more electron-rich, sterically more easily accessible alkene functionality. **e**, Energy transfer sensitization of diverse disulfides yielding the respective hydrothiolated products. **f**, Slight modification of the reaction conditions gives access to arylthioethers (using acetone as solvent). **g**,**i**, Application of this protocol to functionalize drug derivatives and bioconjugates. **h**, Hydrothiolation of alkynes allows the *vic*-di-methylthiolation or construction of sulfur-containing heterocycles. Data are reported as percent isolated yield except **3e**, **3i**, **3l**, **3u**, **3af** and **3aj**, which are reported as ^{1}H NMR yield using CH_2Br_2 as internal standard. Product **3v** was obtained due to rearrangement. Hydrothiolation reactions and the robustness screen were performed once. See Supplementary Section 3.2 for experimental details and characterization data. DCE, 1,2-dichloroethane.

suggests that the reverse reaction, namely rTTEnT (vide infra) definitively takes place. Independent confirmation for the TTEnT rate constant was gathered in phosphorescence lifetime measurements (Supplementary Fig. 12). A k_{TTEnT} of $(1.31 \pm 0.04) \times 10^7\ M^{-1}\ s^{-1}$ is in excellent agreement with the ns-TAS experiments. For determination of the aforementioned k_{rTTEnT} and the underlying equilibrium

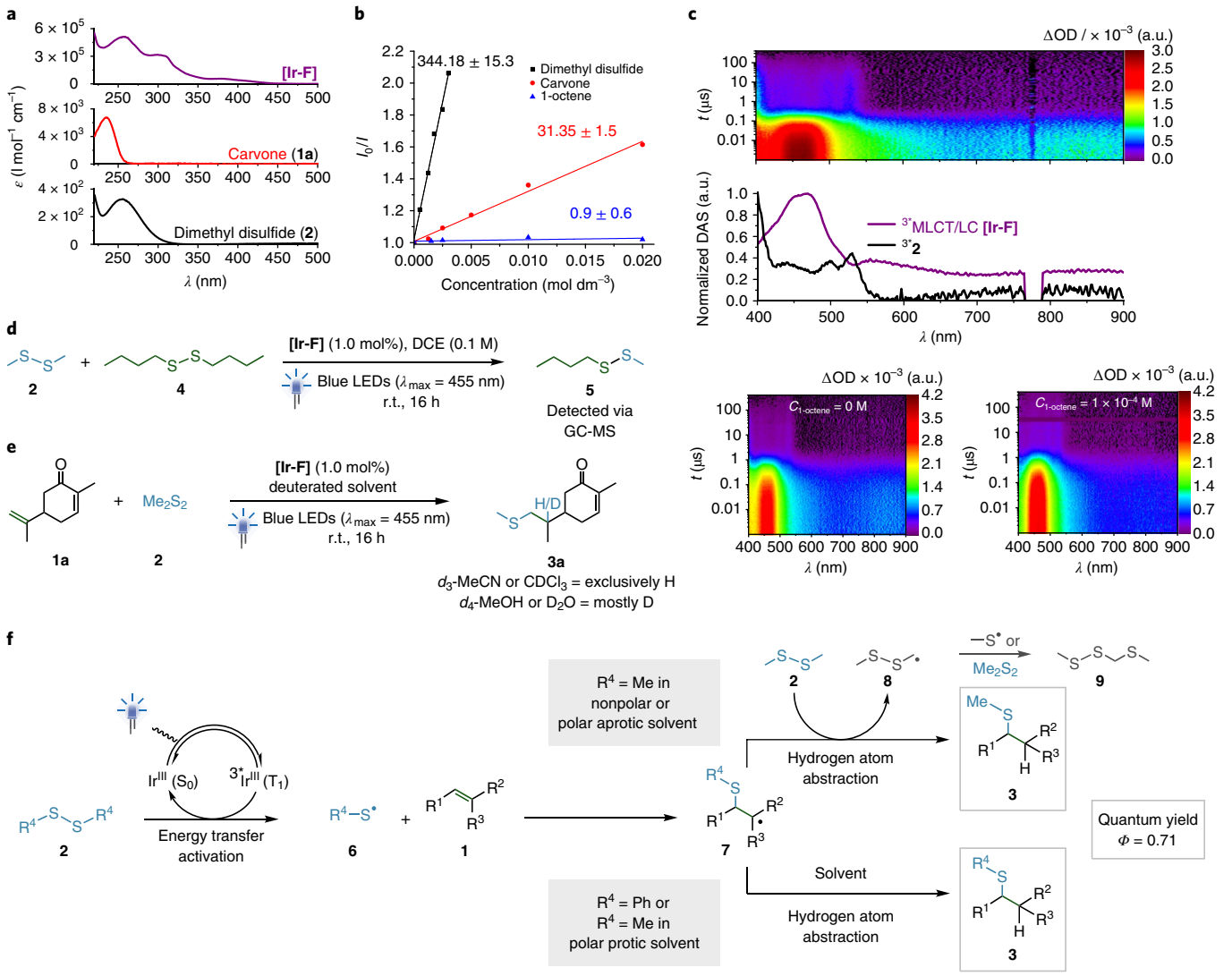

Fig. 4 | Proposed reaction mechanism of the photosensitized disulfide–ene reaction derived from diverse mechanistic studies. a, UV–vis absorption spectroscopy of the individual reaction components shows that the photocatalyst is the only light absorber. **b**, Stern–Volmer quenching studies suggest an energy transfer event between the excited-state photosensitizer and the disulfide ($n = 6$ independent samples (dimethyl disulfide (**2**) and carvone (**1a**)) or $n = 5$ independent samples (1-octene) for the linear regression). **c**, Triplet–triplet sensitization of the disulfide was investigated using ns-TAS to shed light on the reaction kinetics. **d**, A scrambling experiment utilizing two aliphatic disulfides points towards the existence of thiyl radical intermediates. **e**, Depending on the reaction conditions, hydrogen atom abstraction can either take place from the alkyl disulfide or the solvent. **f**, Proposed reaction mechanism of the overall transformation revealed by different spectroscopic as well as additional experiments. Experiments in **a**, **b**, **d** and **e** were all performed once. See Supplementary Information for further details. OD, optical density.

constant K_{TTEnT} we performed ns-TAS experiments with different [**Ir–F**] to **2** ratios. For the

$$^{3*}\text{MLCT/LC}([\mathbf{Ir–F}]) + \mathbf{2} \rightleftarrows [\mathbf{Ir–F}] + {}^{3*}\mathbf{2} \quad (4)$$

equilibrium, $(k_{obs}\text{-}k_{GSR,[Ir–F]})$ for the overall TTEnT relates to[44]

$$(k_{obs} - k_{GSR,[Ir–F]}) = k_{TTEnT} \cdot [[\mathbf{Ir–F}]] + k_{rTTEnT} \cdot [\mathbf{2}] \quad (5)$$

Division by the concentration of **2** results in the following linear expression:

$$\frac{(k_{obs} - k_{GSR,[Ir–F]})}{[\mathbf{2}]} = \frac{k_{TTEnT} \cdot [[\mathbf{Ir–F}]]}{[\mathbf{2}]} + k_{rTTEnT} \quad (6)$$

We took the $(k_{obs}\text{-}k_{GSR,[Ir–F]})/[\mathbf{2}]$ versus $[[\mathbf{Ir–F}]]/[\mathbf{2}]$ plots to derive k_{TTEnT} as $(5.26 \pm 0.23) \times 10^7\,M^{-1}s^{-1}$, k_{rTTEnT} as $(8.65 \pm 0.88) \times 10^6\,M^{-1}s^{-1}$ and K_{TTEnT} as 6.08 ± 0.71. Notably, due to S–S bond weakening and homolytic cleavage to afford thiyl radical intermediates (vide infra), the thermodynamically favoured reverse energy transfer, which reinstates the ^{3*}MLCT/LC state of the [**Ir–F**] photocatalyst, is slowed down.

Having confirmed the triplet sensitization mechanism, the consecutive reaction steps were systematically investigated. To this end, we performed a radical scrambling experiment to investigate the presence of thiyl radical intermediates under our reaction conditions. Irradiation of dimethyl disulfide (**2**) and dibutyl disulfide (**4**) with visible light in the presence of the [**Ir–F**] photocatalyst resulted in methyl butyl disulfide (**5**) as the major product. Very probably, methyl butyl disulfide (**5**) formation involves thiyl radicals as intermediates and their radical recombination or radical addition into another disulfide molecule (Fig. 4d).

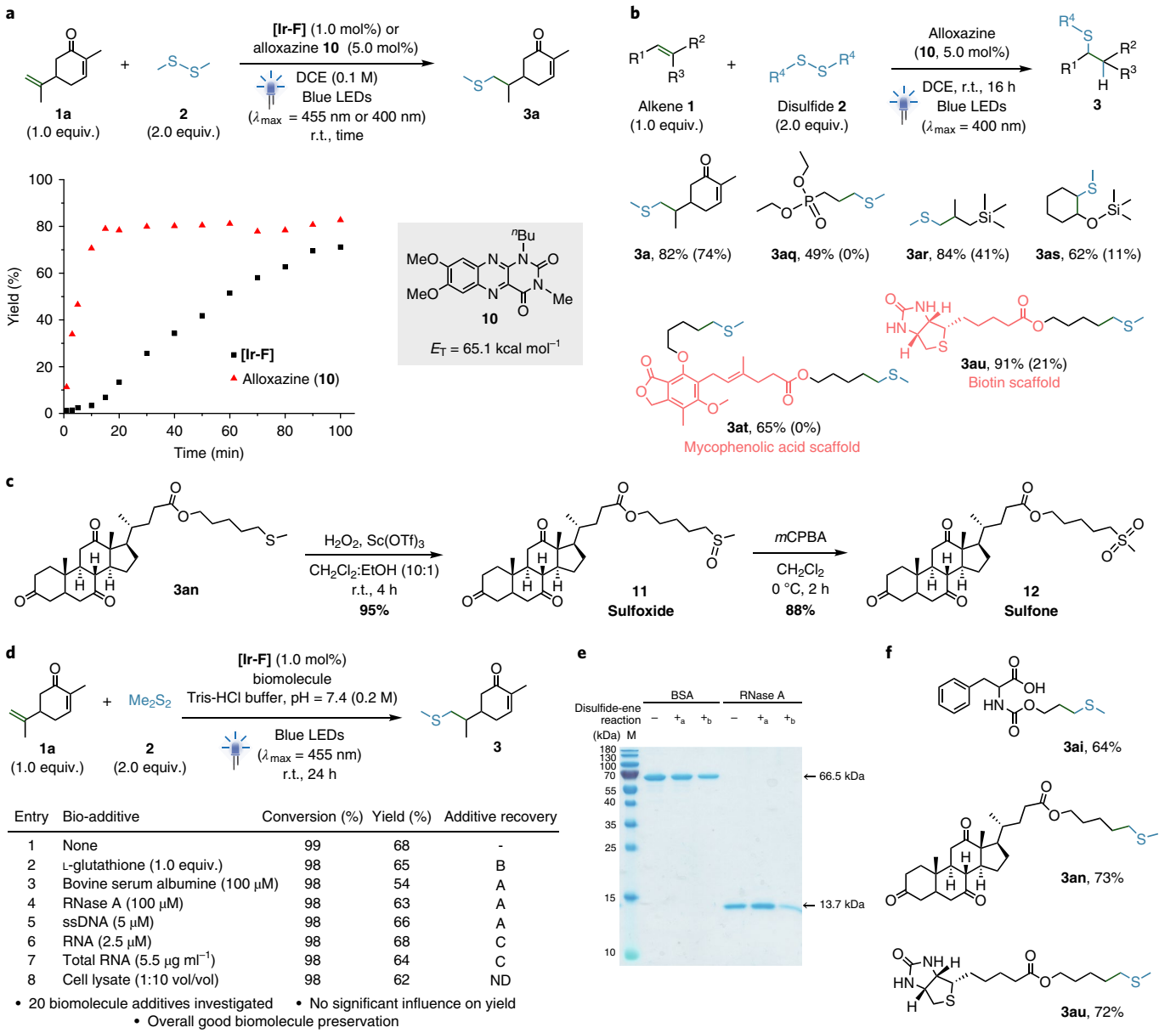

Entry	Bio-additive	Conversion (%)	Yield (%)	Additive recovery
1	None	99	68	-
2	L-glutathione (1.0 equiv.)	98	65	B
3	Bovine serum albumine (100 μM)	98	54	A
4	RNase A (100 μM)	98	63	A
5	ssDNA (5 μM)	98	66	A
6	RNA (2.5 μM)	98	68	C
7	Total RNA (5.5 μg ml^{-1})	98	64	C
8	Cell lysate (1:10 vol/vol)	98	62	ND

- 20 biomolecule additives investigated
- No significant influence on yield
- Overall good biomolecule preservation

Fig. 5 | Improvement of the photocatalytic system based on mechanistic investigation, access to sulfoxides and sulfones by stepwise oxidation of thioethers and biocompatibility screening of the disulfide–ene reaction. a, The previously gained mechanistic understanding has been used for improvement of the catalytic system. By switching to transition-metal-free alloxazine photocatalyst **10**, the reaction rate could be significantly improved. **b**, The improved catalytic system allows the successful hydromethylthiolation of alkenes, which were low-yielding or not reactive using **[Ir-F]** as photosensitizer (**[Ir-F]** yields are stated in parentheses). Reaction conditions: alkene (0.3 mmol, 1.0 equiv.), disulfide (0.6 mmol, 2.0 equiv.), alloxazine (0.015 mmol, 5.0 mol%), DCE (0.1 M), λ_{max} = 400 nm, r.t., 16 h. Data are reported as percent isolated yield except **3ar** and **3as**, which are reported as ^{1}H NMR yield using CH_2Br_2 as internal standard. **c**, The obtained methylthioether products can be stepwise oxidized to pharmaceutically important sulfoxide or sulfone functionalities. **d**, The biocompatibility of the disulfide–ene reaction was investigated by additive-based screening of biomolecules and was performed in cell lysate (A = biomolecule identified, no degradation observed; B = biomolecule identified, some degradation observed; C = biomolecule identified, significant degradation observed; D = no biomolecule identified, complete degradation observed, ND = not determined, a conclusion is not possible). Reduced form of *L*-glutathione was used. **e**, Qualitative analysis of biomolecules by UPLC–MS or gel electrophoresis after irradiation revealed that, in most cases, no degradation occurred, as depicted by the SDS-polyacrylamide gel, indicating preservation of BSA and RNase A (100 μM$_a$ and 10 μM$_b$) under the reaction conditions. **f**, Various alkenes were also successfully hydromethylthiolated in cell lysate. Reaction profile (**a**), hydrothiolation reactions (**b**), follow-up reactions (**c**) and biocompatibility screening experiments (**d** and **f**) were performed once. SDS–PAGE (**e**) was repeated twice with similar results.

Hydrogen atom abstraction in the α-position to the sulfur atom of **2** by carbon-centred radical **7** could lead to the formation of the carbon-centred disulfide radical **8**. This radical consecutively reacts with a methylthiyl radical or another dimethyl disulfide (**2**) molecule to yield trisulfide **9**, which was isolated as a side product during the optimization process. When the reaction was performed in different deuterated polar aprotic or nonpolar solvents, no deuterium incorporation within the product structure was observed, suggesting that the hydrogen atom abstraction is exclusively taking place from the disulfide (Fig. 4e). In contrast, if the reaction was performed in polar protic solvents, almost full deuterium incorporation in the product molecule was detected. Under these reaction

conditions, the polar protic solvent is the hydrogen atom source (Supplementary Section 4.9).

As we succeeded in monitoring the TTEnT from the **[Ir–F]** photocatalyst to dimethyl disulfide (**2**), we turned our attention to probe the final step in the disulfide–ene reaction, namely the reaction of ^{3*}**2** with 1-octene. In this context, the 400 and 440 nm signature of ^{3*}**2** enabled the reaction to be followed spectroscopically. In ns-TAS experiments with 1-octene in a concentration range from 1×10^{-7} to 5×10^{-3} M, the concentration-dependent ^{3*}**2** decay gave rise to $k_{react}=(1.38\pm0.07)\times10^{8}\,M^{-1}\,s^{-1}$. The final thioether product is, however, spectroscopically invisible in the wavelength range from 400 to 1600 nm.

Based on screening, ns-TAS, phosphorescence lifetime quenching and radical scrambling experiments, the following mechanism is proposed (Fig. 4f). After excitation of **[Ir–F]**, a TTEnT activation of dimethyl disulfide (**2**) leads to homolytic S–S bond cleavage, generating corresponding thiyl radical **6**. Similar to the classical thiol–ene reaction, the chemoselective *anti*-Markovnikov addition into the most electron-rich alkene occurs in an irreversible and quick fashion and gives rise to carbon-centred radical **7**. If aliphatic disulfides and polar aprotic or nonpolar solvents are used, **7** abstracts a hydrogen atom from another disulfide molecule **2**, resulting in the formation of product **3** and trisulfide **9**. In contrast, if aryl disulfides in acetone as solvent or aliphatic disulfides in polar protic solvents are reacted, the hydrogen atom abstraction event takes place between carbon-centred radical **7** and the solvent.

Applications and outlook. The mechanistic analysis revealed the occurrence of a Dexter-type TTEnT process, where physical contact between energy acceptor and energy donor is required. We therefore aimed for the improvement of our catalytic system by decreasing the steric bulkiness of the photosensitizer, on the one hand, and increasing its triplet excited-state energy, on the other. Due to its planar shape and its triplet excited-state energy of 65.1 kcal mol^{-1}, organic alloxazine photocatalyst **10** emerged as an ideal candidate[45]. The irradiation wavelength for this catalytic system was adjusted to 400 nm. The transition-metal-free alloxazine-derived photosensitizer might allow transformations not suitable with the **[Ir–F]** catalytic system due to different photo- and electrochemical properties. We validated our hypothesis by running the benchmark reaction between carvone (**1a**) and dimethyl disulfide (**2**) under reaction conditions optimized for the **[Ir–F]**-sensitized protocol, but using alloxazine **10**. Importantly, the desired product was obtained in 62% yield, proving the suitability of the designed catalytic system. After optimizing the reaction conditions, we recorded the reaction profile of this transition-metal-free catalytic system and compared it to the **[Ir–F]**-based system. Due to the increase in triplet excited-state energy and the decrease in steric bulkiness of the photosensitizer, TTEnT is favoured, and, in turn, the reaction is completed within 10 min rather than 90 min (Fig. 5a). All of the aforementioned facts support our mechanistic hypothesis.

With our optimized catalytic system in hand, we focused on the hydromethylthiolation of substrates, which turned out to be low-yielding or unreactive in the **[Ir–F]**-based catalysis (Fig. 5b). Satisfyingly, the yields of some substrates were increased substantially using our improved protocol, for example, hydromethylthiolation of the biotin derivative **3au** was increased by 70% to 91% isolated yield. Moreover, these new conditions enabled the hydromethylthiolation of substrates that could not be transformed using the **[Ir–F]** photocatalyst. For example, methylthiolated phosphonate **3aq** and the mycophenolic acid derivative **3at** were obtained in 49% and 65% yield, respectively.

Any of the alkylthioether products are oxidizable in a stepwise and high-yield manner to the corresponding sulfoxides (**11**) or sulfones (**12**). Both are versatile and important structural motifs in diverse pharmaceuticals or agrochemicals (Fig. 5c)[46,47].

Motivated by the importance of methylthioether scaffolds in biological processes we investigated a biocompatible version of the disulfide–ene reaction potentially suitable for applications in biological systems, such as labelling of biomolecules[48]. Using water with a physiologically compatible Tris-HCl buffer (0.2 M, pH 7.4) as solvent, we probed the biocompatibility of the disulfide–ene reaction of carvone (**1a**) in the presence of 20 biomolecules in an additive-based screening approach (Fig. 5d)[39,40]. Amino acids, saccharides, nucleosides, single-stranded DNA, RNA (short RNA and total RNA) and human cell lysate were among the tested biomolecules. Gratifyingly, the yield of **3a** was not affected by the presence of any of the biomolecules. In most cases, ultra performance liquid chromatography–mass spectrometry (UPLC–MS) and gel electrophoresis analyses documented that the biomolecules were not subject to degradation under the reaction conditions (Fig. 5e and Supplementary Section 8.2). In addition, the disulfide–ene reaction between dimethyl disulfide (**2**) and a variety of olefins was tested in the presence of human cell lysate, containing various endogenous biomolecules (Fig. 5f). Notably, the desired hydromethylthiolated products were formed. Our results indicate that this transformation might be suitable for biological systems, and applications are currently being investigated in our laboratories.

Due to its high atom economy, complete chemo- and regioselectivity, biocompatibility and high synthetic yields, this transformation might be classified as a click reaction, in analogy to the photoinitiated thiol–ene reaction[49]. Remarkably, the TTEnT-enabled disulfide–ene reaction proceeds chemoselectively in the presence of thiols, providing ways and means to a complementary strategy of constructing carbon–sulfur bonds (Supplementary Section 4.12).

Conclusion

In conclusion, we have discovered a photosensitized disulfide–ene click reaction that enables the chemo- and regioselective construction of alkyl- and arylthioethers under remarkably mild and biocompatible reaction conditions. Our protocol allows the chemo- and regioselective incorporation of methylthioether scaffolds into highly complex substrates, as proven by a broad substrate scope and the functionalization of bioconjugates or drug derivatives. The detailed study of the reaction mechanism, with special focus on the TTEnT sensitization process via TAS, has led to the development of an improved and more efficient transition-metal-free catalytic system. We are convinced that the establishment of visible-light-mediated energy transfer activation, based on careful mechanistic analysis and rational design, will open up a new field with versatile applications in organic synthesis, allowing hardly accessible bond (dis)connections.

Data availability. The data supporting the findings of this study are available within the paper and its Supplementary Information, or from the corresponding authors upon reasonable request.

Received: 21 February 2018; Accepted: 29 May 2018;
Published online: 06 August 2018

References

1. Trost, B. M. Selectivity: a key to synthetic efficiency. *Science* **219**, 245–250 (1983).
2. Wender, P. A. & Miller, B. L. Synthesis at the molecular frontier. *Nature* **460**, 197–201 (2009).
3. Takahashi, N. et al. Reactive sulfur species regulate tRNA methythiolation and contribute to insulin secretion. *Nucleic Acids Res.* **45**, 435–445 (2017).
4. Kowalak, J. A. & Walsh, K. A. *β*-methylthio-aspartic acid: identification of a novel posttranslational modification in ribosomal protein S12 from *Escherichia coli*. *Protein Sci.* **5**, 1625–1632 (1996).
5. Forouhar, F. et al. Two Fe–S cluster catalyse sulfur insertion by radical-SAM methylthiotransferases. *Nat. Chem. Biol.* **9**, 333–338 (2013).
6. Stubbe, J. & van der Donk, W. A. Protein radicals in enzyme catalysis. *Chem. Rev.* **98**, 705–762 (1998).

7. Dunbar, K. L., Scharf, D. H., Litomska, A. & Hertweck, C. Enzymatic carbon–sulfur bond formation in natural product biosynthesis. *Chem. Rev.* **117**, 5521–5577 (2017).
8. Kolberg, M., Strand, K. R., Graff, P. & Andersson, K. K. Structure, function, and mechanism of ribonucleotide reductases. *Biochim. Biophys. Acta* **1699**, 1–34 (2004).
9. Fraústo da Silva, J. J. R. & Williams, R. J. P. *The Biological Chemistry of the Elements* (Oxford Univ. Press: New York, NY, 2011).
10. Damani, L. A. *Sulphur-Containing Drugs and Related Organic Compounds* (Wiley: Chichester, 1989).
11. Dénès, F., Pichowicz, M., Povie, G. & Renaud, P. Thiyl radicals in organic synthesis. *Chem. Rev.* **114**, 2587–2693 (2014).
12. Posner, T. Beiträge zur Kenntniss der ungesättigten Verbindungen. II. Ueber die Addition von Mercaptanen an ungesättigte Kohlenwasserstoffe. *Ber. Dtsch. Chem. Ges.* **38**, 646–657 (1905).
13. Hoyle, C. E. & Bowman, C. N. Thiol–ene click chemistry. *Angew. Chem. Int. Ed.* **49**, 1540–1573 (2010).
14. Stenzel, M. H. Bioconjugation using thiols: old chemistry rediscovered to connect polymers with nature's building blocks. *ACS Macro Lett.* **2**, 14–18 (2013).
15. van Dijk, M., Rijkers, D. T. S., Liskamp, R. M. J., van Nostrum, C. F. & Hennink, W. E. Synthesis and applications of biomedical and pharmaceutical polymers via click chemistry methodologies. *Bioconjug. Chem.* **20**, 2001–2016 (2009).
16. Huynh, V. T., Chen, G., de Souza, P. & Stenzel, M. H. Thiol–yne and thiol–ene 'click' chemistry as a tool for a variety of platinum drug delivery carriers, from statistical copolymers to crosslinked micelles. *Biomacromolecules* **12**, 1738–1751 (2011).
17. Lowe, A. B. Thiol–ene 'click' reactions and recent applications in polymer and materials synthesis. *Polym. Chem.* **1**, 17–36 (2010).
18. Tyson, E. L., Ament, M. S. & Yoon, T. P. Transition metal photoredox catalysis of radical thiol–ene reactions. *J. Org. Chem.* **78**, 2046–2050 (2013).
19. Tyson, E. L., Niemeyer, Z. L. & Yoon, T. P. Redox mediators in visible light photocatalysis: photocatalytic radical thiol–ene additions. *J. Org. Chem.* **79**, 1427–1436 (2014).
20. Keylor, M. H., Park, J. E., Wallentin, C.-J. & Stephenson, C. R. J. Photocatalytic initiation of thiol–ene reactions: synthesis of thiomorpholin-3-ones. *Tetrahedron* **70**, 4264–4269 (2014).
21. Chen, Y., Kamlet, A. S., Steinman, J. B. & Liu, D. R. A biomolecule-compatible visible-light-induced azide reduction from a DNA-encoded reaction-discovery system. *Nat. Chem.* **3**, 146–153 (2011).
22. Huang, H., Zhang, G., Gong, L., Zhang, S. & Chen, Y. Visible-light-induced chemoselective deboronative alkynylation under biomolecule-compatible conditions. *J. Am. Chem. Soc.* **136**, 2280–2283 (2014).
23. Nair, D. P. et al. The thiol–Michael addition click reaction: a powerful and widely used tool in materials chemistry. *Chem. Mater.* **26**, 724–744 (2014).
24. Luo, Y.-R. *Handbook of Bond Dissociation Energies in Organic Compounds* (CRC Press: Boca Raton, FL, 2003).
25. Zhao, J., Wu, W., Sun, J. & Guo, S. Triplet photosensitizers: from molecular design to applications. *Chem. Soc. Rev.* **42**, 5323–5351 (2013).
26. Atta, M. et al. The methylthiolation reaction mediated by the radical-SAM enzymes. *Biochim. Biophys. Acta* **1824**, 1223–1230 (2012).
27. Stillwell, W. G. Methylthiolation: a new pathway of drug metabolism. *Trends Pharmacol. Sci.* **2**, 250–252 (1981).
28. Ciamician, G. The photochemistry of the future. *Science* **36**, 385–394 (1912).
29. Prier, C. K., Rankic, D. A. & MacMillan, D. W. C. Visible light photoredox catalysis with transition metal complexes: applications in organic synthesis. *Chem. Rev.* **113**, 5322–5363 (2013).
30. Twilton, J. et al. The merger of transition metal and photocatalysis. *Nat. Rev. Chem.* **1**, 0052 (2017).
31. Skubi, K. L., Blum, T. R. & Yoon, T. P. Dual catalysis strategies in photochemical synthesis. *Chem. Rev.* **116**, 10035–10074 (2016).
32. Metternich, J. B. & Gilmour, R. Photocatalytic *E*→Z isomerization of alkenes. *Synlett* **27**, 2541–2552 (2016).
33. Lu, Z. & Yoon, T. P. Visible light photocatalysis of [2+2] styrene cycloadditions by energy transfer. *Angew. Chem. Int. Ed.* **51**, 10329–10332 (2012).
34. Blum, T. R., Miller, Z. D., Bates, D. M., Guzei, I. A. & Yoon, T. P. Enantioselective photochemistry through Lewis acid-catalyzed triplet energy transfer. *Science* **354**, 1391–1395 (2016).
35. Welin, E. R., Le, C., Arias-Rotondo, D. M., McCusker, J. K. & MacMillan, D. W. C. Photosensitized, energy transfer-mediated organometallic catalysis through electronically excited nickel(II). *Science* **355**, 380–385 (2017).
36. Hopkinson, M. N., Gómez-Suárez, A., Teders, M., Sahoo, B. & Glorius, F. Accelerated discovery in photocatalysis using a mechanism-based screening method. *Angew. Chem. Int. Ed.* **55**, 4361–4366 (2016).
37. Teders, M., Gómez-Suárez, A., Pitzer, L., Hopkinson, M. N. & Glorius, F. Diverse visible-light-promoted functionalizations of benzotriazoles inspired by mechanism-based luminescence screening. *Angew. Chem. Int. Ed.* **56**, 902–906 (2017).
38. Benati, L., Montevecchi, P. C. & Spagnolo, P. Free-radical reactions of benzenethiol and diphenyl disulphide with alkynes. Chemical reactivity of intermediate 2-(phenylthio)vinyl radicals. *J. Chem. Soc. Perkin Trans.* **1**, 2103–2109 (1991).
39. Collins, K. D. & Glorius, F. A robustness screen for the rapid assessment of chemical reactions. *Nat. Chem.* **5**, 597–601 (2013).
40. Gensch, T., Teders, M. & Glorius, F. Approach to comparing the functional group tolerance of reactions. *J. Org. Chem.* **82**, 9154–9159 (2017).
41. Snyder, J. J., Tise, F. P., Davis, R. D. & Kropp, P. J. Photochemistry of alkenes. 7. *E–Z* isomerization of alkenes sensitized with benzene and derivatives. *J. Org. Chem.* **46**, 3609–3611 (1981).
42. Lowry, M. S. et al. Single-layer electroluminescent devices and photoinduced hydrogen production from an ionic iridium(III) complex. *Chem. Mater.* **17**, 5712–5719 (2005).
43. Murov, S. L., Carmichael, I. & Hug, G. L. *Handbook of Photochemistry* 2nd edition (Marcel Dekker, New York, 1993).
44. Guldi, D. M., Neta, P. & Asmus, K.-D. Electron-transfer reactions between C_{60} and radical ions of metaloporphyrins and arenes. *J. Phys. Chem.* **98**, 4617–4621 (1994).
45. Mojr, V. et al. Tailoring flavins for visible light photocatalysis: organocatalytic [2+2] cycloadditions mediated by a flavin derivative and visible light. *Chem. Commun.* **51**, 12036–12039 (2015).
46. Feng, M., Tang, B., Liang, S. H. & Jiang, X. Sulfur containing scaffolds in drugs: synthesis and application in medicinal chemistry. *Curr. Top. Med. Chem.* **16**, 1200–1216 (2016).
47. Devendar, P. & Yang, G. F. Sulfur-containing agrochemicals. *Top. Curr. Chem.* **375**, 82 (2017).
48. Shieh, P. & Bertozzi, C. R. Design strategies for bioorthogonal smart probes. *Org. Biomol. Chem.* **12**, 9307–9320 (2014).
49. Kolb, H. C., Finn, M. G. & Sharpless, K. B. Click chemistry: diverse chemical function from a few good reactions. *Angew. Chem. Int. Ed.* **40**, 2004–2021 (2001).

Acknowledgements

The authors thank K. Gottschalk, L. Roling, S. Hüwel, W. Dörner and S. Wulff for experimental and technical assistance and R. Honeker, L. Candish and Z. Nairoukh for helpful discussions (all WWU Münster). This work was supported by the Deutsche Forschungsgemeinschaft (Leibniz Award to F.G. and RE2796/6-1 to A.R.) and by the Fonds der Chemischen Industrie (doctoral fellowship to L.A. and Dozentenpreis to A.R.). M.T. thanks SusChemSys 2.0 for general support.

Author contributions

M.T., F.S.-K., A.G.-S., R.K. and F.G. designed, performed and analysed the catalytic and mechanistic experiments. C.H., A.K. and D.G. designed, performed and analysed transient absorption data and related spectroscopic mechanism studies. L.A. and M.T. designed and performed the biocompatibility screening experiments. M.T., C.H., L.A., F.S.-K., A.R., D.G. and F.G. prepared the manuscript, with contributions from all authors.

Additional information

Supplementary information is available for this paper at https://doi.org/10.1038/s41557-018-0102-z.

Reprints and permissions information is available at www.nature.com/reprints.

Correspondence and requests for materials should be addressed to D.G. or F.G.

Publisher's note: Springer Nature remains neutral with regard to jurisdictional claims in published maps and institutional affiliations.

nature research

Corresponding author(s): Dirk Guldi and Frank Glorius

Reporting Summary

Nature Research wishes to improve the reproducibility of the work that we publish. This form provides structure for consistency and transparency in reporting. For further information on Nature Research policies, see Authors & Referees and the Editorial Policy Checklist.

Statistical parameters

When statistical analyses are reported, confirm that the following items are present in the relevant location (e.g. figure legend, table legend, main text, or Methods section).

n/a	Confirmed	
☐	☒	The exact sample size (*n*) for each experimental group/condition, given as a discrete number and unit of measurement
☐	☒	An indication of whether measurements were taken from distinct samples or whether the same sample was measured repeatedly
☒	☐	The statistical test(s) used AND whether they are one- or two-sided *Only common tests should be described solely by name; describe more complex techniques in the Methods section.*
☒	☐	A description of all covariates tested
☒	☐	A description of any assumptions or corrections, such as tests of normality and adjustment for multiple comparisons
☒	☐	A full description of the statistics including central tendency (e.g. means) or other basic estimates (e.g. regression coefficient) AND variation (e.g. standard deviation) or associated estimates of uncertainty (e.g. confidence intervals)
☒	☐	For null hypothesis testing, the test statistic (e.g. *F*, *t*, *r*) with confidence intervals, effect sizes, degrees of freedom and *P* value noted *Give P values as exact values whenever suitable.*
☒	☐	For Bayesian analysis, information on the choice of priors and Markov chain Monte Carlo settings
☒	☐	For hierarchical and complex designs, identification of the appropriate level for tests and full reporting of outcomes
☒	☐	Estimates of effect sizes (e.g. Cohen's *d*, Pearson's *r*), indicating how they were calculated
☒	☐	Clearly defined error bars *State explicitly what error bars represent (e.g. SD, SE, CI)*

Our web collection on statistics for biologists may be useful.

Software and code

Policy information about availability of computer code

Data collection	No software was used for data collection.
Data analysis	Regression analysis (linear regression) and processing of reaction profiles, luminescence and UV/vis spectra was performed using Microsoft Excel 2013 or Origin 2016. UPLC-MS analysis was performed utilizing Bruker Compass DataAnalysis 4.4 for data analysis. Transient absorption spectroscopy data was evaluated using the TIMP based GloTarAn program. GC-MS spectra were analysed using the Agilent MSD Productivity ChemStation software. Electrochemistry data analysis was performed using Metrohm Autolab - Nova 1.10 software.

For manuscripts utilizing custom algorithms or software that are central to the research but not yet described in published literature, software must be made available to editors/reviewers upon request. We strongly encourage code deposition in a community repository (e.g. GitHub). See the Nature Research guidelines for submitting code & software for further information.

Data

Policy information about availability of data

All manuscripts must include a data availability statement. This statement should provide the following information, where applicable:

- Accession codes, unique identifiers, or web links for publicly available datasets
- A list of figures that have associated raw data
- A description of any restrictions on data availability

All data is made available in the Supplementary Information. Raw data is available from the corresponding authors upon reasonable request.

Field-specific reporting

Please select the best fit for your research. If you are not sure, read the appropriate sections before making your selection.

☒ Life sciences ☐ Behavioural & social sciences ☐ Ecological, evolutionary & environmental sciences

For a reference copy of the document with all sections, see nature.com/authors/policies/ReportingSummary-flat.pdf

Life sciences study design

All studies must disclose on these points even when the disclosure is negative.

Sample size	No statistical methods were used to predetermine sample size. Verification of the reaction methodology was performed exhaustively by scope preparation and by the performance of an additive-based robustness screen.
Data exclusions	No data were excluded from the analysis.
Replication	Newly reported reactions were repeated and / or performed by several of the authors. All attempts at replication were succesful. Spectroscopic data could be reproduced with similar results. Furthermore, the use of diverse spectroscopic techniques confirmed the observed kinetic rate constants. During the whole study, no replication problems were observed.
Randomization	In our study, an energy transfer enabled hydroalkylthiolation of diverse alkenes and alkynes is described. Consecutively, as part of the design, mechanistic analysis, scope preparation and biocompatibility assesment, radomization is not relevant to this study (methodology paper).
Blinding	The study describes the design and the mechanistic analysis of a novel hydroalkylthiolation methodology. Only in vitro samples were tested. As part of the study, no blinding was necessary.

Reporting for specific materials, systems and methods

Materials & experimental systems

n/a	Involved in the study
☒	☐ Unique biological materials
☒	☐ Antibodies
☐	☒ Eukaryotic cell lines
☒	☐ Palaeontology
☒	☐ Animals and other organisms
☒	☐ Human research participants

Methods

n/a	Involved in the study
☒	☐ ChIP-seq
☒	☐ Flow cytometry
☒	☐ MRI-based neuroimaging

Eukaryotic cell lines

Policy information about cell lines

Cell line source(s)	Cell lines were obtained from Sigma (HeLa).
Authentication	Cells lines were purchased and not authenticated.
Mycoplasma contamination	All cell lines used were tested negative for mycoplasma contamination.

Commonly misidentified lines (See ICLAC register)	No commonly misidentified cell lines were used.